TEMEL-ij
Technology | Engineering | Management | Entrepreneurship | Learning | International Journal

STUDY OF PHYSICAL PROCESSES IN THE CATHODE REGION OF A WELDING ARC

Manahil Tongov[1], Alexander Gechev[2]

Abstract: *The study presents results from mathematical modelling of the physical processes in the cathode area of an electric welding arc with tungsten cathode. Finite Element Method (FEM) is used to solve electrical, thermal and fluid tasks. When solving the equations, the characteristics of the materials involved in the process are set as temperature functions. As a result of simulation modelling the cathode voltage drop, temperature fields, electric potential, and current density close to the cathode have been obtained. The methods of reading the heat balance in the cathode region are discussed and the role of plasma cooling for concentrating the current lines through the electrode tip is shown.*

***Key words**: FEM, TIG, Thermal Plasma, Thermal Processes, Electrical Processes*

1. INTRODUCTION.

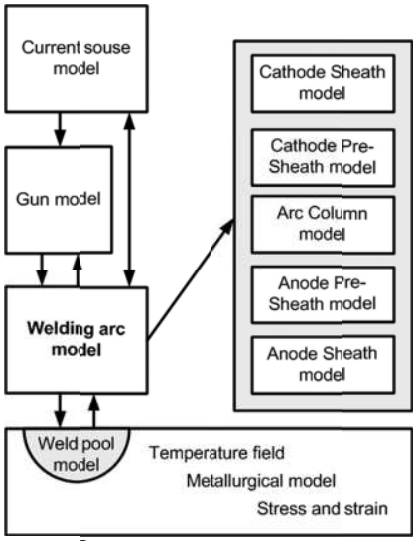

Fig.1. General scheme of modeling the process of arc welding

The mathematical modelling of the processes during welding with non-consumable electrode (TIG and plasma arc welding) is an exceptionally complicated process associated with solving a number of tasks (fig.1). It is usually assumed that the welding power source maintains a stable current or changes it according to a certain program during pulsed arc processes. The same applies to the flow rate of the used gases. In the welded workpiece, a thermal and/or deformation equations are typically solved to determine the thermal cycles, temporary and residual stresses. Usually, the influence of the welding arc on the workpiece is reduced to the usage of a specific heat source distributed over the surface of the workpiece (Gaussian distribution is commonly used) or in a specific volume (fig.2). Also, in some studies the welding arc and the weld pool are modelled simultaneously, and usually data is given about the depth and shape of the penetration [1, 2].

Modelling the processes in the welding arc is done in three different ways. The first approach is to examine the movement of plasma particles and the reactions between them [3]. The second is to model the processes by solving thermal, electric and fluid equations [4 ÷ 9] and also electromagnetic equations [4 ÷ 7, 9]. In this case, in addition to the differential equations, analytical dependencies on the concentration, temperature, and electron and ion velocities necessary to determine the electron and ionic currents are often used. The third approach involves solving the differential equations used in the previous two cases [10].

[1] M. Tongov, Assoc. Prof. PhD, Faculty of Industrial Technology, Technical University – Sofia (tongov@tu-sofia.bg)
[2] A. Gechev, Ass., Faculty of Industrial Technology, Technical University – Sofia (a_gechev@tu-sofia.bg)

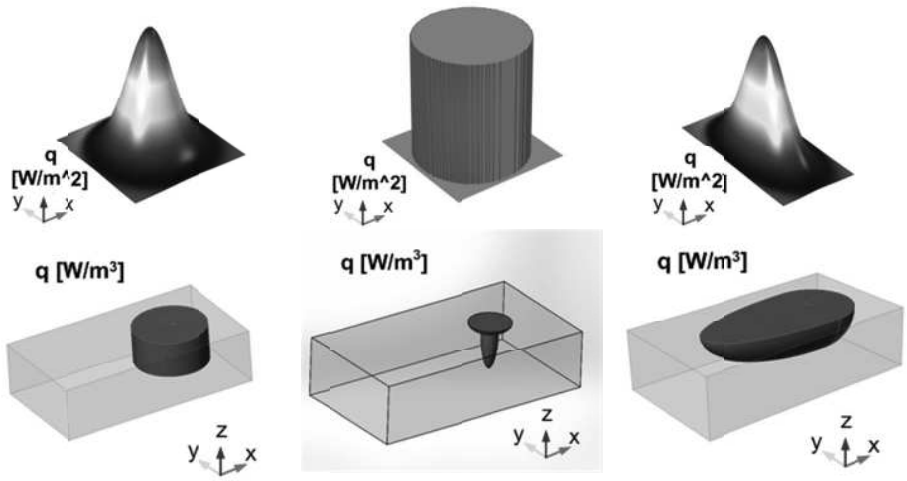

Fig.2. Examples of thermal sources used to model the interactions between the welding arc and the workpiece

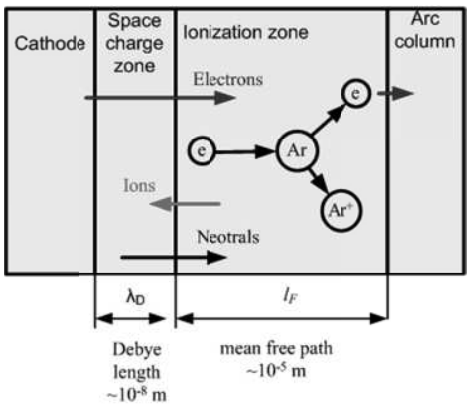

Fig.3. Subarreas in cathode region

When modelling the processes in the cathode region, it is often divided into two sub areas (fig. 3). The first one, which is in direct contact with the cathode, has a small size (in the order of the Debby length) and inside, interactions between the particles does not happen. The second is between the first and the arc column and is an ionization zone (the size is from several micrometers to 0.1 [mm]) and there are considered mainly the processes between charged particles. For these interactions, cross section data about the reactions in the argon plasma are used [3, 11 ÷ 13].

2. MODEL DESCRIPTION.

The diagram shown in Figure 4 is used to realize the model. In the framework of this study, the following equations were solved: thermal for determining the temperatures in the electrode and the plasma; Fluid for determining the gas phase velocities that affect the temperature distribution; electrical to determine the current density and, respectively, the power of the volumetric heat source. All material characteristics are set as temperature functions and the equations are solved for a cylindrical coordinate system[3].

To solve the fluid problem, the continuity and the Navier-Stokes equations for compressible fluid are used:

$$\frac{\partial \rho_{Ar}}{\partial t} + \nabla.(\rho \mathbf{u}) = 0 \qquad (1)$$

$$\rho_{Ar}\frac{\partial \mathbf{u}}{\partial t} + \rho_{Ar}\mathbf{u}.\nabla\mathbf{u} = -\nabla p + \nabla.\left(\mu\left(\nabla\mathbf{u} + (\nabla\mathbf{u})^T\right) - \frac{2}{3}\mu(\nabla.\mathbf{u})\mathbf{I}\right) \qquad (2)$$

Here $\boldsymbol{\rho}_{Ar}$ is the argon density, [kg/m^3]; μ - the dynamic viscosity, [Pa.s], $\mathbf{I}$ - the single tensor and $\mathbf{u}$ is the velocity vector, [m/s]. The boundary conditions are shown in figure 4.

Calculating the temperature is reduced to solving the solving the differential equations:

In the electrode

[3] The coupled problem is stationary but time dependant solution is used as a first stet because of highly nonlinearity of the equations used to find consistent initial values for second stationary step.

$$\rho_W C_{pW} \frac{\partial T}{\partial t} = \nabla.(\nabla T) + q_e \quad (3)$$

In argon

$$\rho_{Ar} C_{pAr} \frac{\partial T}{\partial t} + \rho_{Ar} C_{pAr} \mathbf{u}.\nabla T = \nabla.(\nabla T) + q_e - q_{rad} \quad (4)$$

where ρ_W and ρ_{Ar} are respectively the densities of the tungsten and argon, [kg/m^3]; C_{pW} *and* C_{pAr} - specific heat capacities at constant pressure, [J/(kg.K)]; q_e and q_{rad} respectively are the heat output emitted as a result of current flow and plasma radiation, [W/m^3].

The boundary conditions are shown in figure 5, the plasma interaction with the cathode being discussed below.

The following equations are used to solve the electrical task:

$$-\nabla.(\sigma \nabla V) = Q \quad (5)$$

$$\mathbf{E} = \nabla V \quad (6)$$

$$\mathbf{J} = \sigma \mathbf{E} \quad (7)$$

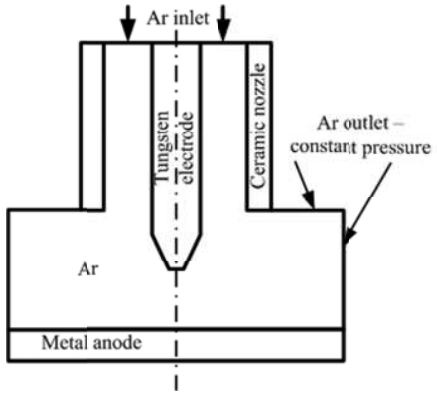

Fig. 4. Geometry schematic and fluid flow boundary conditions.

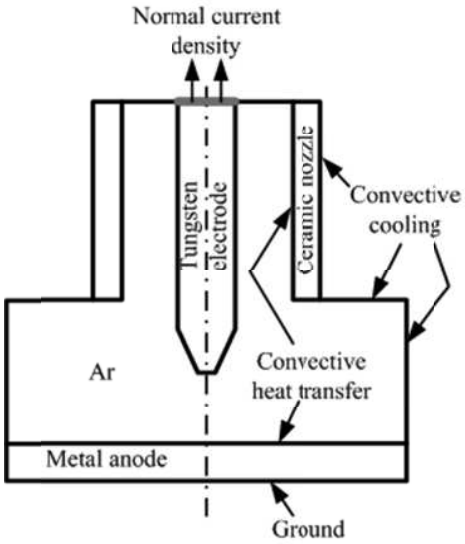

Fig.5. Thermal boundary conditions

Here σ is the argon electrical conductivity [S/m]; Q - the space charge density, [C/m^3]; V - electric potential [V]; $\boldsymbol{E}$ - the electrical field vector, [V/m]; $\boldsymbol{J}$ -the current density vector, [A/m^2]. The boundary conditions are shown in Figure 5 (the remaining surfaces are electrically insulated).

The modeling of the processes in the cathode region is carried out as follows. Depending on the cathode temperature, the emission of electrons is limited according to Richardson's equation, [A/m^2]

$$j_R = \beta A T^2 \exp\left(-\frac{\varphi}{kT}\right) \quad (8)$$

where β is a material-dependent coefficient (for tungsten according to [14] it's valued 0.5); T - the absolute temperature of the cathode surface; k – Boltzmann's constant; φ - work function (for tungsten alloyed with thorium φ = 2.65 [eV]) and A - quantum coefficient, defined as $A = \left(4\pi m_e k^2 e\right)/h^3$. Here m_e and e are the mass and charge of the electron, and h is the Planck's constant.

The strength of the electric field in front of the cathode affects the emitted current (Schottky effect). This influence is accounted for by the reduction of the work function for the electron emission with the value

$$\Delta\varphi = \sqrt{\frac{e^3 E_n}{4\pi\varepsilon_r\varepsilon_0}} \qquad (9)$$

where ε_r is the relative dielectric permeability of argon (for argon $\varepsilon_r \approx 1$); ε_0 - the dielectric permeability of the vacuum; E_n - the electric field strength component on the normal to the cathode surface (fig. 6) and

$$\begin{aligned} AB &\Rightarrow \quad E_n = E_z \\ BC &\Rightarrow \quad E_n = -E_r\cos(\alpha) + E_z\sin(\alpha) \\ CD &\Rightarrow \quad E_n = -E_r \end{aligned} \qquad (10)$$

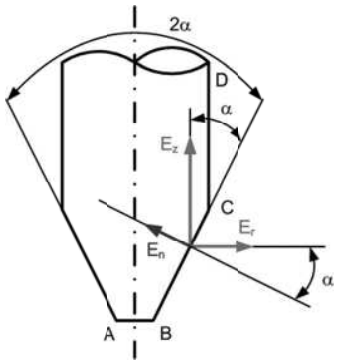

Fig.6. Determination of the normal component of the electric field strength

The effective value of the work function is defined as $\varphi_{eff} = \varphi - \Delta\varphi$. From equations (6) and (7) we obtain the limit for the emission current with the Schottky effect

$$j_{R-S} = \beta A T^2 \exp\left(-\frac{\varphi}{kT}\right).\exp\left(\frac{1}{kT}\sqrt{\frac{e^3 E_n}{4\pi\varepsilon_0}}\right) \qquad (11)$$

The current density across the cathode surface is j_n. It can be determined in a way similar to the determination of the electric field strength:

$$\begin{aligned} AB &\Rightarrow \quad j_n = j_z \\ BC &\Rightarrow \quad j_n = -j_r\cos(\alpha) + j_z\sin(\alpha) \\ CD &\Rightarrow \quad j_n = -j_r \end{aligned} \qquad (12)$$

In the cathode region there is an electron (j_e) and an ion (j_i) current. In [4] it is quoted by [15] dependence derived from the energy balance in the cathode region connecting these two currents, the ionization potential (U_i) and the cathode voltage drop (U_C). Using this dependence it is obtained that $j_i = j_e\left(U_C/U_i\right)$. When we consider that $j_n = j_e + j_i$, and also the limitation for the electron current we get

$$j_e = j_n\frac{U_i}{U_i + U_C} \qquad j_i = j_n\frac{U_C}{U_i + U_C} \qquad (13)$$
$$j_e \le j_{R-S}$$

The cooling effect of electron emission is determined by the effective work function and the emission current. When the ions reach the surface of the cathode they recombine. This process also requires the emission of an electron. Therefore, the cooling effect should also take into account this process. This means that the total cooling flow resulting from the electron emission is

$$q_{C-e} = j_n\frac{(\varphi - \Delta\varphi)}{e} \qquad (14)$$

The electrons that enter the plasma bring energy into it. The heat flux to the plasma can be determined by the emission current and the temperature of the cathode T_C (the electrons that interact with the ions are not accounted for) as [4]:

$$q_{p-e} = j_e\frac{2kT_C}{e} \qquad (15)$$

The latter equation is based on the fact that electrons obey Maxwell's distribution. But in the cathode (temperature does not exceed 3500 [K]) the distribution of Fermi - Dirac is in effect. In addition, the electron emission is from the Fermi level but we will be not discus this problem now.

When ions reach the surface of the cathode, they recombine and energy is released eU_i. This energy is released by γ quantum and the plasma is actually transparent to it. This means that the plasma loses this energy. In equation (4), we measure the radiation of the plasma through the heat flux q_{rad} and it should not be duplicated. At the same time, the probability that this photon is directed to the cathode surface is 50%. Part of the photons are reflected - we account for it with a reflection

coefficient (ε_m). In the first approximation, this coefficient is equal to the degree of cathode surface emissivity. In this case, the surface of the cathode will be heated and the density of this heat flux is

$$q_{C-emi} = \frac{1}{2}\varepsilon_m j_i U_i \quad (17)$$

The ions reaching the cathode interact with it, and some of their kinetic energy is transmitted to the cathode surface. Under the cathode voltage drop U_C within the cathode region the ions acquire additional kinetic energy equal to eU_C (assuming that only primary ionization is observed). Part of this energy (taken into account by the coefficient ε_k, as we have assumed ε_k = 1 in this study) they give to the cathode

$$q_{C-U_C} = \varepsilon_k j_i . U_C \quad (18)$$

The rest of the energy increases the energy state of plasma in the cathode region. Thus, the thermal flux cooling the surface of the plasma in the contact area is

$$q_{p-U_C} = \varepsilon_k j_i U_C - (1-\varepsilon_k) j_i . U_C = (2\varepsilon_k - 1) j_i U_C \quad (19)$$

Neutral atoms are also heating the cathode. This process can be described as convection with a heat flow q_{conv}. For the heat flux that is heating the surface of the cathode we obtain:

$$q_C = -q_{C-e} + q_{C-emi} + q_{C-U_C} + q_{conv}$$

and for the heat flux to the plasma

$$q_p = q_{p-e} - q_{p-U_C} - q_{conv}$$

By replacing the heat fluxes in these equations we obtain:

$$q_C = -j_n \frac{\varphi - \Delta\varphi}{e} + \frac{1}{2}\varepsilon_m j_i U_i + \varepsilon_k j_i U_C + \alpha(T_{Ar} - T_s) \quad (20)$$

$$q_p = j_e \frac{2kT_C}{e} - (2\varepsilon_k - 1) j_i U_C - \alpha(T_{Ar} - T_C) \quad (21)$$

where α is the coefficient of surface heat transfer, [W/(m^2.K)].

In order for the equations (17) and (18) to be used as boundary conditions, the cathode voltage drop must be determined. This can be done by any of the formulas known in the literature or by the potential field obtained by solving the electrical task. When using the second method, it is necessary to know the size of the cathode region. We assume that it is equal to the ion mean free path (l_F), depending on local temperature and density. We determine it by the number of particles in unit volume (n_0) and the cross section of the interaction (S) $l_F = (n_0 S)^{-1}$. The number of particles in a unit volume is determined by the argon density (ρ_{Ar}), depending on pressure and temperature, and the atomic mass (m_{Ar} = 39.95 [g/mol]) $n_0 = \rho_{Ar} N_A m_{Ar}^{-1}$. The cross section of the interaction is calculated as $S = \pi(r_i + r_{eff})^2$, where r_i = 154 [pm] is the effective radius of the ion, and r_{eff} is the mean radius of the surrounding particles $r_{eff} = ((1-\chi) r_{Ar} + \chi . r_i)$. Here χ is the degree of ionization in the cathode region, and r_{Ar} = 71 [pm] is the radius of the atom of argon.

That's how we obtain

$$l_F = \frac{m_{Ar}}{\pi \rho_{Ar} N_A ((1-\chi) r_{Ar} + (1+\chi) r_i)^2} \quad (22)$$

For every point of the boundary between the cathode and the plasma, the cathode voltage drop (fig. 7), which is used in the equations (11, 17 and 18), is determined

To solve the equations included in the model it is necessary to specify the characteristics of the materials. They are shown in Fig. 8 - Fig.18 [16÷24].

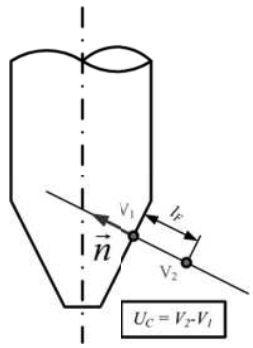

Fig.7. Cathode drop determination

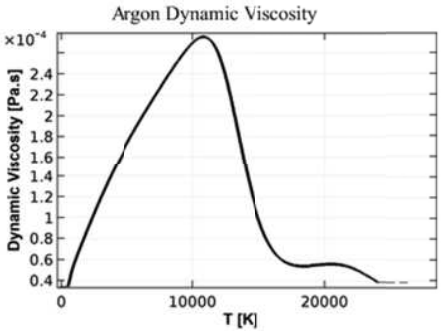

Fig.8.

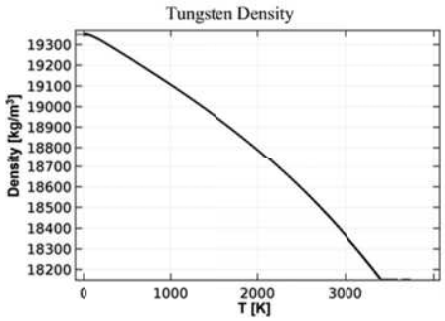

Fig.9.

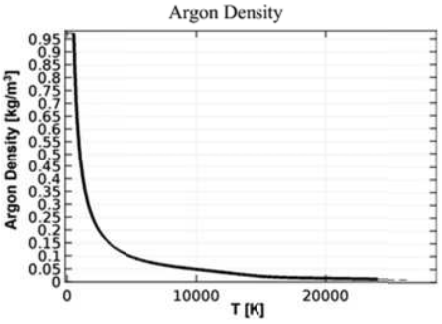

Fig.10.

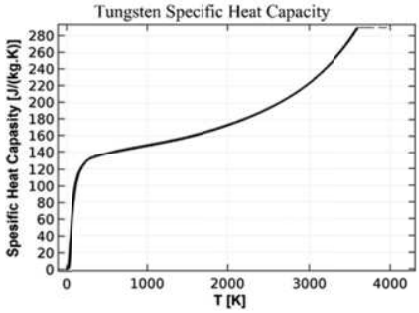

Fig.11.

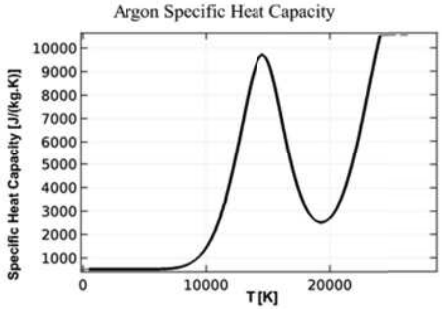

Fig.12

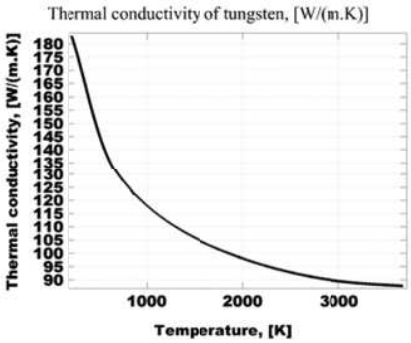

Fig.13

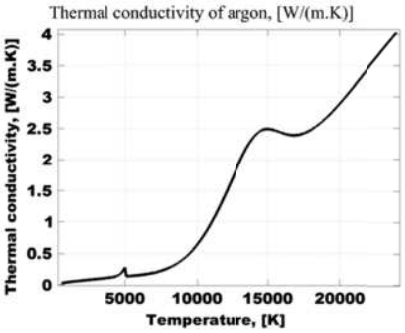

Fig.14

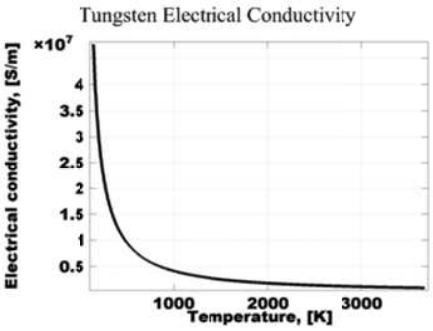

Fig.15

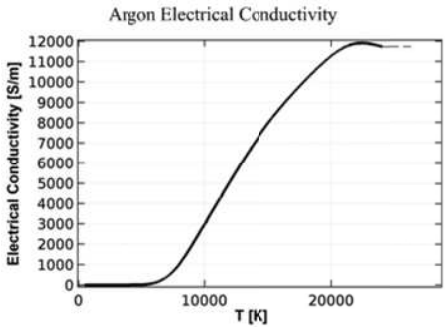

Fig.16

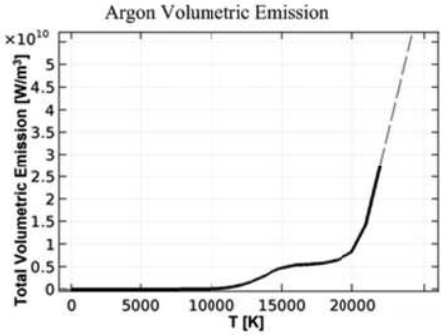

Fig.17

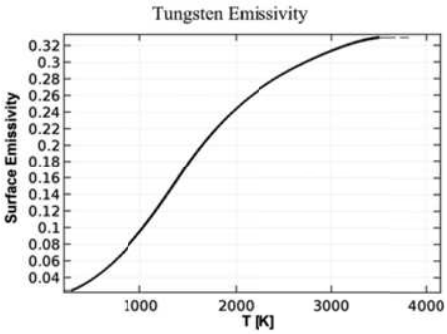

Fig.18

3. DISCUSSION AND ANALYSIS

When solving the model, an electrode with a diameter of 4 [mm], a sharpening angle of $2\alpha=30^0$ and a radius of the area AB 0.2[mm] is used. The flow rate of argon is 6 [l/min] and the inside diameter of the gas nozzle 16 [mm]. The length of the arc is 2[mm] and the length of the electrode with respect to the gas nozzle is 8 [mm]. The welding current is 125 [A].

Figure 19 shows the temperature field in the argon near the tungsten electrode. The maximum plasma temperature is in the range of 13500 [K], with the maximum values located along the arc axis but distant from the end of the electrode. Throughout the contact area between the electrode and the plasma, large temperature gradients are observed. This can be judged by the temperature along the arc axis (fig.20). In addition, the temperature goes through a maximum, due to cooling, because of fluid movement. On the surface of the cathode, the plasma temperature is 6000 [K], but we must point out that it is different for different points on the surface of the cathode. The curve indicating the velocity of the fluid along the arc axis also passes through a maximum (fig.21) and reaches a value of 0.52 [m/s]. By comparing the last two figures, it can be concluded that the range of maximum temperatures is limited by the fluid flow. At the same time, the speeds directly below the electrode are negligible - of the order of 25 [mm/s].

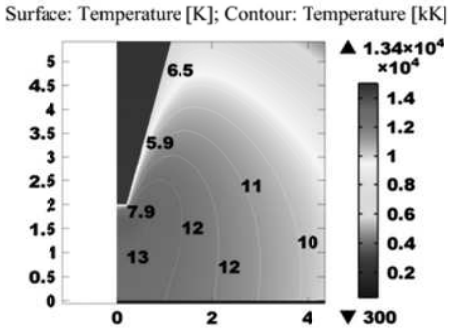

Fig.19. Temperature field.

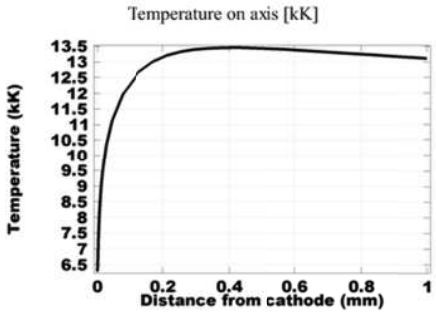

Fig.20. Temperature fn arc axis.

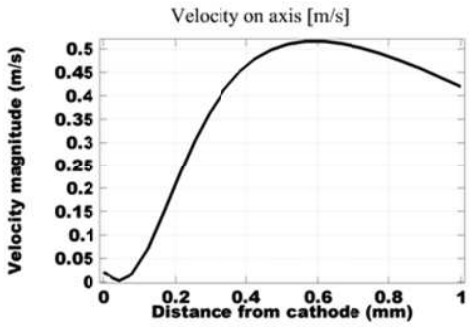

Fig.21. Gas velocity on arc axis.

The surface temperature of the cathode and the plasma temperature along the cathode border are shown in Figure 22. By moving away from the end of the electrode along the cathode surface the temperatures decrease and at some point the protective gas already has a cooling effect on it. In the area of low cathode temperatures and protective gas there is no current flowing from the electrode to the plasma because of its low emissivity and the high resistance of the gas phase due to the extremely low degree of ionization.

The electric field is illustrated in fig. 23, showing the distribution of the potential and the equipotential lines for the current density. As expected, the maximum current density is obtained at the tip of the electrode. Fig. 24 shows the variation of the electric field strength along the arc axis.

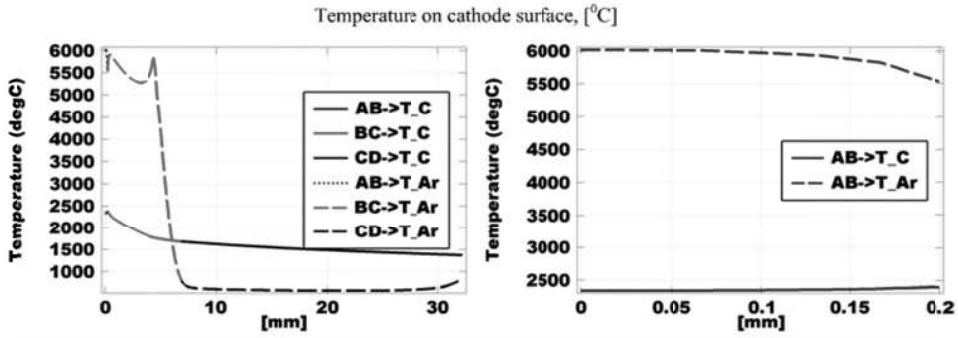

Fig.22. Temperatures on tungsten – argon boundary

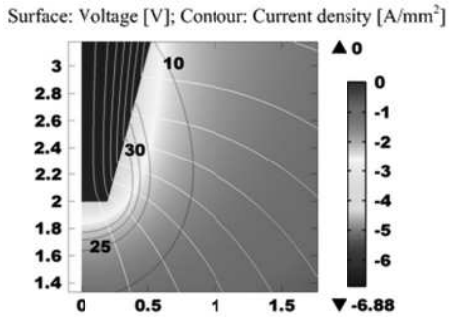

Fig.23. Electric field

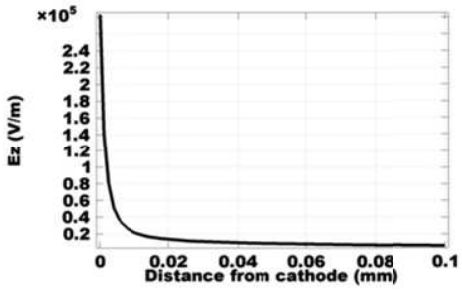

Fig.24. Electric field strength along the arc axis (axial component)

The change in the electric field strength is most significant in the immediate vicinity of the cathode surface. Then, going further into the ionization zone, it decreases, which corresponds to the volumetric charge. This zone is less than the length of ion mean free path and is smaller than the size of the cathode area. The approximate size of this area is 10 [μm] and is considerably larger than λ_D. Here we have to point out that no conclusions can be made regarding the ionization zone with the model that we are considering. To analyze the processes in this zone, a detailed model based on particle motion and their interactions is required. Fig. 25 shows how the electric potential changes along the arc axis, and in fig. 26 the graphs for the variations of the potential in front of the tip of the tungsten electrode are shown.

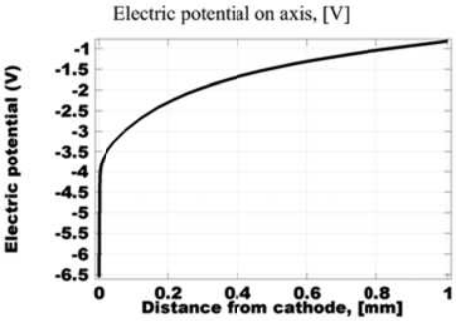

Fig.25. Electric potential changes along the arc axis

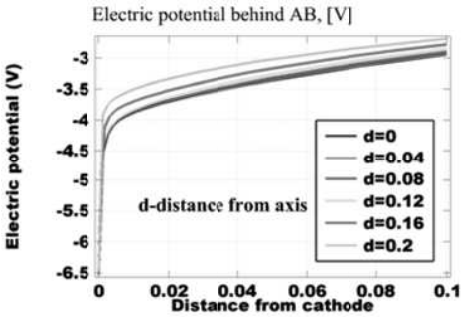

Fig.26. Electric potential in front of the tip of the tungsten electrode

In accordance with the change in field strength, the electrical potential also changes sharply in the proximity of the cathode. From fig. 24 and fig. 25 it can be concluded that there is no change of the characteristics of the said graphs, which clearly shows the size of the cathode region – it means that the transition from the zone of ionization to the arc column is smooth. Also, in front of the face of the cathode, which has a radius of 0.2 [mm] in the case in question, there is no significant difference in the change in electrical potential. Immediately beneath the tungsten electrode, the current flow conditions are practically the same, and the cathode voltage drop in this area is the same.

Significantly different is the situation on the inclined surface of the electrode (fig.27). By moving away from point B to 2 [mm], the potential increases at a constant distance from the surface of the electrode, and then decreases. When this decrease begins, the field strength along the electrode surface normal changes and the area with a sharp change of electric potential disappears.

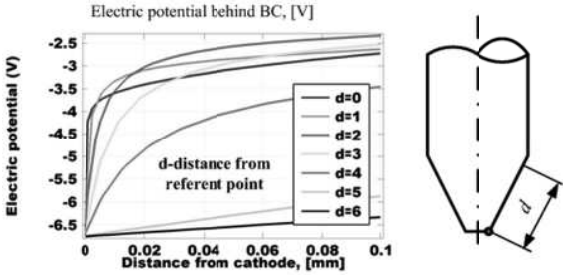

Fig.27. Electric potential in front of conic surface of the tungsten electrode

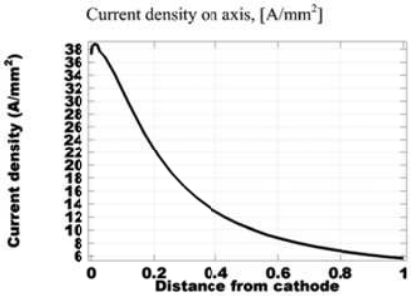

Fig.28. Current density along the arc axis

The current density along the arc axis is shown in Fig.28. It is largest immediately below the electrode and decreases with distancing from its surface due to the current dissipation because of the conductivity of the argon and the influence of the anode.

4. CONCLUSIONS

The results obtained by this computer simulation of the processes in the cathode region during welding with a tungsten electrode are relevant to this case, but the approach used is applicable to solving a wider range of TIG and plasma arc welding models. The main conclusions that can be drawn are:

1. A model is proposed, involving simultaneous solving of electrical, thermal and fluid tasks in welding conditions concerning a non-consumable electrode.
2. At the boundary between the cathode and the plasma, heat flows are used as boundary conditions, taking into account the interactions between the charged particles and the surface of the cathode, and the plasma.
3. Results for the temperature and electric field near the cathode surface are presented.
4. The cathode voltage drop along the surface of the electrode is presented.

5. REFERENCES

[1] Lu F., X. Tang, H. Yu, S. Yao, Numerical simulation on interaction between TIG welding arc and weld pool, Computational Materials Science 35 (2006) 458–465p.
[2] Mochizuki M., M. Tanaka, S. Okano, Integrated simulation model between arc plasma process and weld mechanics toward accurate distortion analysis, Transactions of JWRI, Special Issue on WSE 2011(2011), 123-128p.
[3] Dowdent J., P. Kapadiat and B. Fenn, Space charge in plasma arc welding and cutting, J. Phys. D Appl. Phys. 26 (1993) 1215-1223
[4] Wendelstorf J., Ab inito modelling of thermal plasma gas discarges (elecric arc), Disertation, 2000
[5] Meng J., X. Dong, Numerical Simulation and Analysis on Jet Characteristics of Combined Plasma Arc, The Open Mechanical Engineering Journal, 2011, 5, 78-86
[6] Choquet I., H. Nilsson, M. Sass-Tisovskaya, Modeling and simulation of a heat source in electric arc welding.
[7] Murphy A., M. Tanaka, K. Yamamoto, S. Tashiro, J. Lowke, CFD modelling of arc welding –the importance of the arc plasma, Seventh International Conference on CFD in the Minerals and Process Industries CSIRO, Melbourne, Australia, 9-11 December 2009
[8] Traidia A., F. Roger, A. Chidley, J. Schroeder and T. Marlaud, Effect of Helium-Argon Mixtures on the Heat Transfer and Fluid Flow in Gas Tungsten Arc Welding, J. Chem. Chem. Eng. 5 (2011) 854-861p.
[9] Bauchire J., E. Langlois-Bertrand1, C. Izarra, Numerical Modelling of a Free-Burning Arc in Argon. A Tool for Understanding the Optical Mirage Effect in a TIG Welding Device, Proceedings of the COMSOL Conference 2009 Milan
[10] Aithala S. M., V. Subramaniam, Numerical model of a transferred plasma arc, Journal of Applied Physics, Volume 84, Number 7, 1998
[11] Uhrlandt D., M. Baeva, A. V. Pipa, R. Kozakov, G. Gött, Cathode fall voltage of TIG arcs from a non-equilibrium arc model, Weld World (2015) 59:127–135
[12] Jose Luis Tapia Fabela, Joel Osbaldo Pacheco-Sotelo, Marquidia Pacheco Pacheco, Jorge Samuel Bentez-Read, Regulo Lopez-Callejas, et al.. Modeling the Voltage Drop Across the Cathode Sheath in HPS. IEEE Transactions on Plasma Science, Institute of Electrical and Electronics Engineers, 2007, 35 (4), pp.1104-1110. <10.1109/TPS.2007.902125>. <hal-00188969>
[13] A. Boutaghane, K. Bouhadef, F. Valensi, S. Pellerin, Y. Benkedda. Theoretical model and experimental investigation of current density boundary condition for welding arc study. The European Physical Journal Applied Physics, 2011, 54 (1), <10.1051/epjap/2011100146>. <hal-00687330>
[14] Кузнецов М. С., Технология получения высокоэмиссионных материалов на основе гексаборида лантана в режиме самораспространяющегося высокотемпературного синтеза при механоактивации шихты, Диссертация на соискание ученой степени кандидата технических наук, 2016
[15] Benilov M.S., A. Marota, A model of cathode region of atmospheric pressure arcs, J. Phis. D: Appl. 28 (1995), 1869-1822.
[16] Shanping Lu, Wenchao Dong, Dianzhong Li, Yiyi Li, Numerical study and comparisons of gas tungsten arc properties between argon and nitrogen,Computational Materials Science 45 (2009) 327–335
[17] Зиновьев В. Е., Теплофизические свойства металлов и сплаввов при высоких температурах. Справочник, М. Металургия, 1989,
[18] E. W. Lemmon and R. T Jacobsenp Viscosity and Thermal Conductivity Equations for Nitrogen, Oxygen, Argon, and Air, International Journal of Thermophysics, Vol. 25, No. 1, January 2004 (© 2004)
[19] H. N. Olsen, Thermal and Electrical Properties of an Argon Plasma, Physics of Fluids 2, 614 (1959); doi: http://dx.doi.org/10.1063/1.1705962
[20] V. A. Baturin, Electrical conductivity of an argon plasma in a stabilized arc, Journal of Applied Mechanics and Technical Physics March 1970, Volume 11, Issue 2, pp 338–346
[21] G.J. Dunn and T.W. Eagar, Calculation of Electrical and Thermal Conductivities of Metalurgical Plasmas, WRC Bulletin 357

https://hypertextbook.com/facts/2004/DeannaStewart.shtml
http://www-ferp.ucsd.edu/LIB/PROPS/PANOS/w.html
http://thermalinfo.ru

ACKNOWLEDGEMENTS

The presented study was possible thanks to a contract: ДН 07/26.